Decarbonizing semiconductor manufacturing: cost-competitiveness of PV-based green hydrogen production

Smart Energy 19 (2025) 100192

Contents lists available at ScienceDirect

Smart Energy

journal homepage: www.journals.elsevier.com/smart-energy

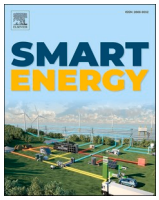

Decarbonizing semiconductor manufacturing: cost-competitiveness of PV-based green hydrogen production

Davide Trapani *, Paolo Marocco, Marta Gandiglio, Massimo Santarelli

Department of Energy, Politecnico di Torino, Corso Duca degli Abruzzi 24, 10129, Torino, Italy

ARTICLE INFO

Keywords:
Hydrogen
Power-to-hydrogen
Optimal design
Hard-to-abate industry
Decarbonization

ABSTRACT

Hard-to-abate industries heavily depend on fossil fuels and low-cost fossil-based feedstocks, significantly contributing to energy-related CO_2 emissions. Therefore, a cost-effective transition towards low-carbon solutions becomes imperative. This study investigates the cost-competitiveness of decarbonizing semiconductor manufacturing by switching from conventional grey hydrogen supply to on-site green hydrogen production in a power-to-hydrogen (P-t-H) system. A silicon wafer production facility with an annual hydrogen demand of approximately 110 tonnes is considered as a case study. An optimization framework based on a metaheuristic approach is developed for the cost-optimal design of the P-t-H system, while the ε-constraint technique is applied to investigate multiple decarbonization targets. The findings indicate that fully relying on grey hydrogen remains the most cost-effective strategy, resulting in a levelized cost of hydrogen (LCOH) of 4 €/kg but emitting 1045 tonnes of CO_2 annually. As grey hydrogen consumption is limited to reduce CO_2 emissions, the LCOH increases exhibiting distinct trends. For decarbonization targets up to 70 %, the LCOH steadily rises to 6.10 €/kg, while stricter CO_2 emissions constraints cause a steeper increase in the hydrogen production cost, reaching 10.51 €/kg in the fully decarbonized scenario. Achieving complete decarbonization requires scaling up the P-t-H components, particularly the pressurized storage tank, which becomes essential for a reliable hydrogen supply. Grid electricity import can prevent the system oversizing, thus boosting the cost-competitiveness of green hydrogen production. Conventional hydrogen supply remains cost-efficient for grey hydrogen purchase prices up to 6 €/kg, while above this threshold integrating on-site green hydrogen production becomes beneficial.

1. Introduction

In 2022 the industry sector directly released 9.2 Gt_{CO2}, contributing to one-quarter of the global energy-related carbon dioxide (CO_2) emissions. In particular, heavy industries in chemical, steel and cement productions were the largest CO_2 emitters generating approximately 6 Gt_{CO2} [1]. Industrial activities were also responsible for around 6.8 Gt_{CO2} in indirect emissions due to heat and electricity imports [2].

The decarbonization of the industry sector is thus crucial to tackle the climate crisis and meet the net-zero emissions target by 2050. However, industrial processes are usually hard-to-abate due to the lack of mature and cost-competitive low-carbon technologies. Moreover, the need to replace or retrofit the existing production plants poses additional techno-economic barriers [2].

The use of green hydrogen is widely considered as a promising strategy for mitigating carbon emissions in different industrial sectors [3]. It has indeed the potential to replace unabated fossil-based hydrogen in traditional industrial applications (e.g., refining, ammonia synthesis and steelmaking) and it can represent a sustainable alternative to fossil fuels in high-temperature heat generation (e.g., glass production and ceramics manufacturing). It is noteworthy that hard-to-abate industries consumed more than 97 Mt of fossil-based hydrogen in 2023 [4]. Specifically, the refining sector was the largest hydrogen consumer with approximately 700 refineries worldwide utilizing over 43 Mt of hydrogen for the hydrocracking and desulfurization processes [4]. Chemical industries required 48.6 Mt of hydrogen as a feedstock for ammonia and methanol synthesis, while steelmaking consumed 5.4 Mt as reducing agent in the direct reduced iron (DRI) process [4]. Hydrogen was also used in specialized industrial applications (i.e., global annual demand of around 1 Mt) such as floating glass production, electronics manufacturing and metal processing [4].

At present, large industries usually opt for on-site production while industrial plants with lower demand mainly rely on merchant hydrogen. In both cases, well-established and low-cost steam methane reforming

* Corresponding author.
E-mail address: davide.trapani@polito.it (D. Trapani).

https://doi.org/10.1016/j.segy.2025.100192
Received 21 March 2025; Received in revised form 27 June 2025; Accepted 27 June 2025
Available online 29 June 2025

(SMR) and coal gasification still dominate hydrogen production. However, due to the notable carbon intensity of these processes (i.e., around 9 kg_{CO2eq}/kg_{H2} for methane and 18 kg_{CO2eq}/kg_{H2} for coal [5]), the identification of alternative production routes is required. Sustainable power-to-hydrogen (P-t-H) systems can effectively contribute to decarbonize hard-to-abate industries by producing hydrogen through renewable-based water electrolysis.

The rising interest in exploiting green hydrogen to reduce industrial carbon emissions is confirmed by the numerous studies available in literature. Moradpoor et al. [6] assessed the techno-economic feasibility of producing green hydrogen for an oil refinery in Finland. They explored the combination of different electrolyzer technologies and renewable power supply schemes, such as power purchase agreement (PPA), newly installed wind turbine and national grid. The PPA-based configuration (with pay as produced scheme and electricity price of 29 €/MWh) with alkaline electrolyzer exhibited the lower production cost while the grid-based scenario proved to be strongly affected by the electricity price volatility. Gandhi et al. [7] explored the adoption of renewable hydrogen in the refining sector of the United Arab Emirates, concluding that in the short-term natural gas prices of around 12 $/MMBtu or carbon prices of 120 $€/t_{CO2}$ are required to enable a cost-effective decarbonization of oil refineries. Al-Subaie et al. [8] investigated different hydrogen production pathways for a refining plant in Ontario (Canada). In particular, the authors compared the cost and the life cycle emissions of generating hydrogen through SMR or grid-connected electrolyzer. Fossil-based hydrogen is confirmed to be the cheapest solution due to technology maturity and low natural gas prices. Conversely, green hydrogen can drastically reduce CO_2 emissions, but to achieve cost-competitiveness, a carbon tax over $\$100/t_{CO2}$ and oxygen valorization are needed (even when it is produced importing grid electricity at 14.3 $/MWh). However, the valorization of by-product oxygen remains hindered by the increased system complexity for compression and storage [9,10]. Moreover, the availability of low-cost conventional oxygen production pathways (e.g., cryogenic distillation and pressure swing adsorption) and the site-specific demand further limit its cost-effectiveness [11,12]. IRENA has recognized the use of green hydrogen as a valid option for the synthesis of low-carbon methanol, despite the resulting production cost ranges between 800 and 1600 $/t [13]. These cost projections were confirmed by Gu et al. [14], who carried out a techno-economic assessment of a green methanol production plant in China. The levelized cost of methanol (LCOM) was found to be 895 €/t, indicating that a carbon price of 65 $€/t_{CO2}$ was needed to break even with the coal-based production route. These results are in line with those reported by Sollai et al. [15], who determined an LCOM of 960 €/t for a similar plant in Italy. Nevertheless, these production costs almost doubled the international market price (around 450 €/t) and revealed that e-methanol is currently far from commercial maturity. Green hydrogen is expected to be pivotal in decarbonizing also ammonia synthesis, despite the persistent cost gap with conventional production routes [16]. Indeed, fossil-based ammonia typically exhibits production costs in the range of 200–500 $\$/t_{NH3}$ [17,18], primarily driven by natural gas prices and carbon pricing mechanisms [19]. Conversely, IRENA reported the current costs of green ammonia between 720 and 1400 $\$/t_{NH3}$ [20], in line with the findings from other recent studies. Specifically, Osman et al. [21] calculated a levelized cost of ammonia (LCOA) of 718 $\$/t_{NH3}$ for a large-scale plant including also a desalination unit. Mingolla et al. [16] assessed renewable ammonia production costs in the range 700–1200 $€/t_{NH3}$, while Nami et al. [22] estimated LCOA of 700 and 950 $€/t_{NH3}$ when adopting alkaline and solid oxide electrolyzer (SOE) technologies, respectively. Similarly, Magnino et al. [19] determined renewable ammonia production costs of 1174 and 1368 $€/t_{NH3}$ for SOE- and PEM-based configuration, respectively. At present, the cost-competitiveness of green ammonia is mainly hindered by the electricity supply price and the electrolyzer investment cost, thereby requiring capital cost reduction and more stringent carbon pricing [19,22]. Nevertheless, a significant cost reduction is projected for 2030 and 2050 with renewable ammonia reaching 480 and 310 $\$/t_{NH3}$, respectively [20]. Similar cost trends are confirmed by Wang et al. [23], who assessed the ammonia production cost in 2030 for different locations in Australia finding values in the range 370–430 $\$/t_{NH3}$. However, Smith et al. [24] identified some potential barriers to be overcome for integrating renewable hydrogen in the traditional process for ammonia production. The methane-fed Haber-Bosch process is indeed optimized and highly thermal integrated; thus, several modifications have to be implemented in the plant layout to synthetize green ammonia (e.g. heat management). Moreover, the existing production facilities are designed to operate in steady-state conditions at nearly full capacity. The exploitation of intermittent renewable energy sources (RES) thus requires the installation of storage systems or the improvement of flexibility in the synthesis loop. Nevertheless, Martinez Alonso et al. [25] highlighted that, despite being more expensive, green hydrogen-based ammonia can represent a more resilient strategy in the short term since its production cost is decoupled from the natural gas price, which has recently experienced sharp variations.

According to the International Energy Agency (IEA), the green hydrogen-based steelmaking is projected to cover 15 % of the primary steel production by 2050 leading to an estimated global demand of approximately 12 Mt of green hydrogen [26]. Vogl et al. [27] analyzed a green H_2-based DRI plant and concluded that cost-competitiveness with conventional blast furnace-basic oxygen furnace (BF-BOF) route can be achieved at renewable electricity costs of 20 €/MWh or carbon prices of 34–68 $€/t_{CO2}$. Bhaskar et al. [28] compared BF-BOF and H_2-based DRI for primary steel production in Norway. They found that using green hydrogen causes an increase of 40 % in steel production cost, resulting in a carbon mitigation cost of up to 180 $\$/t_{CO2}$. Elsheikh and Eveloy [29] investigated the integration of a PV-grid P-t-H system in a DRI-based steelmaking plant in Spain, observing a 74 % reduction in CO_2 emission intensity compared to the conventional BF-BOF route. Superchi et al. [30] examined an innovative small-scale steel mill with a constant hydrogen demand of 285 kg/h. They reported that the carbon intensity of the steelmaking process can be reduced by 84 % by relying on hydrogen produced through electrolysis. Marocco et al. [31] pointed out the need of decarbonizing also the high temperature heat generation in secondary steel production. The authors analyzed a real case study in northern Italy and proved that hydrogen can be cost-effective in reducing the direct emissions of the plant.

Röben et al. [32] evaluated the techno-economic feasibility of installing a power-to-hydrogen system to curb CO_2 emissions in copper production. They confirmed the crucial role of the electricity price in achieving a cost-efficient decarbonization when hydrogen is used as reducing agent and high-temperature heat source. In addition, they emphasized the importance of exploiting by-product oxygen to boost the profitability of this solution. High temperature heat (1450–1650 °C) is also required for the melting phase in the glass production process [33]. Gärtner et al. [34] thus investigated the integration of a power-to-hydrogen system in a German glass industry and determined that a 60 % emission reduction can be obtained when relying on renewable electricity. The role of hydrogen in glass manufacturing was also assessed by Boudries et al. [35], who focused on floating glass production using a protective atmosphere consisting of 90 % nitrogen and 10 % hydrogen. They concluded that, given the abundant solar potential (i.e., $\geq$5 kWh/m^2/day for more than six months per year), on-site hydrogen generation from PV electricity can represent a sustainable solution for a real glass production facility in Algeria.

Although the literature has widely examined the use of green hydrogen in hard-to-abate industries, the potential exploitation of this solution in electronics manufacturing is still to be specifically addressed. Currently, semiconductor industries adopt high purity hydrogen (i.e., $\geq$99.999 %) as a gas carrier in the epitaxial growth of silicon wafers. Rochlitz et al. [36] reported that 500 epitaxy reactors across Europe annually consume around 1.47 kt of fossil-based hydrogen, which is

either delivered by trailers (as compressed gas or liquid) or locally produced through SMR. Replacing the conventional hydrogen supply with on-site production through electrolysis deserves to be investigated as it enables a massive reduction in CO_2 emissions (from SMR and from trailers fuel) without affecting the semiconductor manufacturing process. In this framework, the present work assesses the cost-competitiveness of installing a renewable power-to-hydrogen system in a silicon wafer production plant. The case study examines a semiconductor production facility located in Southern Europe, for which the hourly hydrogen demand profile is available. The assessment aims to investigate the economic competitiveness of PV-based green hydrogen production compared to grey hydrogen supply (i.e., the solution currently adopted). To this end, an optimization framework was developed to address the optimal design of the hydrogen production system. A metaheuristic method was adopted to perform the optimization process and different decarbonization targets were explored by applying the ε-constraint technique. Moreover, to enhance the accuracy of the electrolyzer modeling, both efficiency curve and size-dependent cost function were taken into account.

The structure of this work is as follows: Section 2 describes the optimization framework including the definition of the objective function and the modeling of the system components. The main sizing results are shown and discussed in Section 3 and the conclusions of the study are summarized in Section 4.

2. Methodology

2.1. System layout and operation

The renewable power-to-hydrogen system shown in Fig. 1 includes monocrystalline photovoltaic panels (PV), an electrolyzer (EL), a compression unit (CP), a pressurized hydrogen storage tank (HT), a grey hydrogen back-up system (HBS), an hydrogen purification system to achieve 5.0 grade and a connection to the national electrical grid (GR).

In the schematic layout in Fig. 1, a 5.0 hydrogen purifier is included for completeness. However, this study assumes that the purifier is already installed in the existing industrial configuration. In addition, since the purifier is required in both supply scenarios considered - merchant grey hydrogen delivery and on-site renewable hydrogen production - it does not influence the comparative assessment. For these reasons, the hydrogen purifier is not modeled in detail.

An energy management strategy (EMS) was developed to simulate the operation of the power-to-hydrogen system with hourly resolution over a reference year. A 1 h time step was selected as it ensures a good trade-off between results accuracy and computational cost [37].

The implemented control strategy determines the operating conditions of the system based on the hydrogen demand of the industrial plant and the power production from renewable energy sources (PV in the present case). At each time step, when the hydrogen demand results larger than zero, the EMS identifies the following priority of intervention for the hydrogen supply: first green hydrogen directly from the electrolyzer (if electricity from RES is available), then green hydrogen from the pressurized storage tank and finally grey hydrogen from the fossil-based back-up system. Specifically, the following operating strategies can be distinguished:

- If PV power is available and sufficient to operate the electrolyzer within its modulation range, the electrolyzer is switched on and its production directly serves the industrial plant. Two distinct scenarios can then be identified depending on the balance between hydrogen production and demand:
  - o If hydrogen production exceeds the demand, the surplus is compressed and stored for future use. Any excess PV electricity is then exported to the electrical grid.
  - o If hydrogen production does not meet the demand, the deficit is first covered by resorting to the green hydrogen storage and then by using the grey hydrogen back-up system.
- If PV power is unavailable (e.g., at night) or insufficient to operate the electrolyzer within its modulation range, the electrolyzer is not activated and the demand is entirely covered by the green hydrogen storage and, if needed, by the grey hydrogen back-up system.

Conversely, when there is no hydrogen consumption, any available renewable electricity from the PV is used to produce hydrogen, which is stored until the green hydrogen storage is full. Any remaining excess PV power is then sold to the electrical grid. The detailed logical block diagram is reported in Appendix A.

2.2. Optimal sizing

The proposed optimization framework is shown in Fig. 2, which summarizes the main input data, the optimal sizing methodology and the key performance indicators (KPIs).

The required input data include the hourly hydrogen demand of the industrial plant, the meteorological data for estimating the normalized hourly PV power production, and the techno-economic parameters of the components (e.g., efficiency curve, operating conditions, lifetime, capital expenditure, operational, maintenance and replacement costs). The levelized cost of hydrogen (LCOH) was considered as objective function of the optimization problem, while the sizes of the main components of the power-to-hydrogen systems were set as decision variables (PV, EL, HT). The main outcomes of the design tool include the sizes of the components, the scheduling of the system over the reference year and some techno-economic and environmental KPIs (e.g., cost of

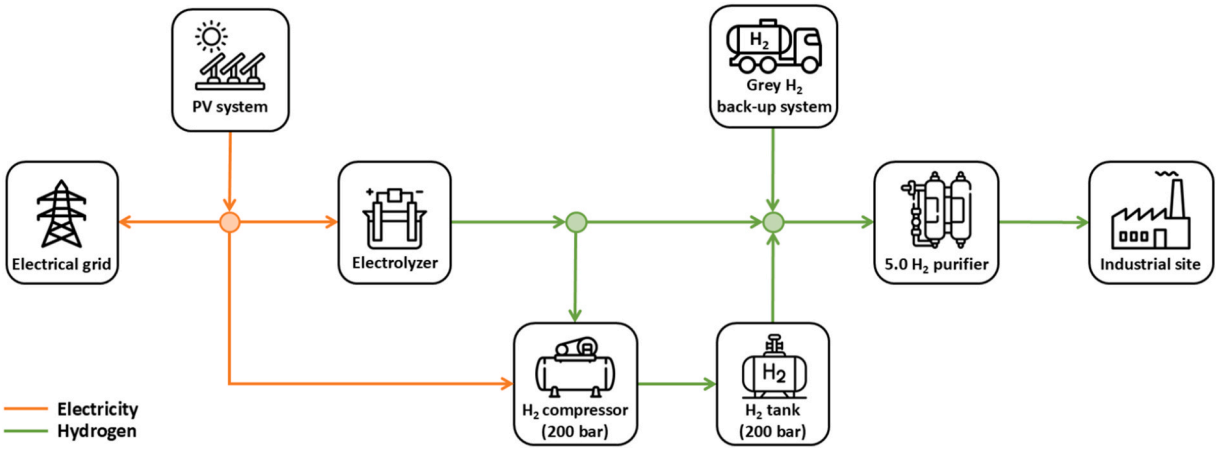

Fig. 1. Power-to-hydrogen system layout.

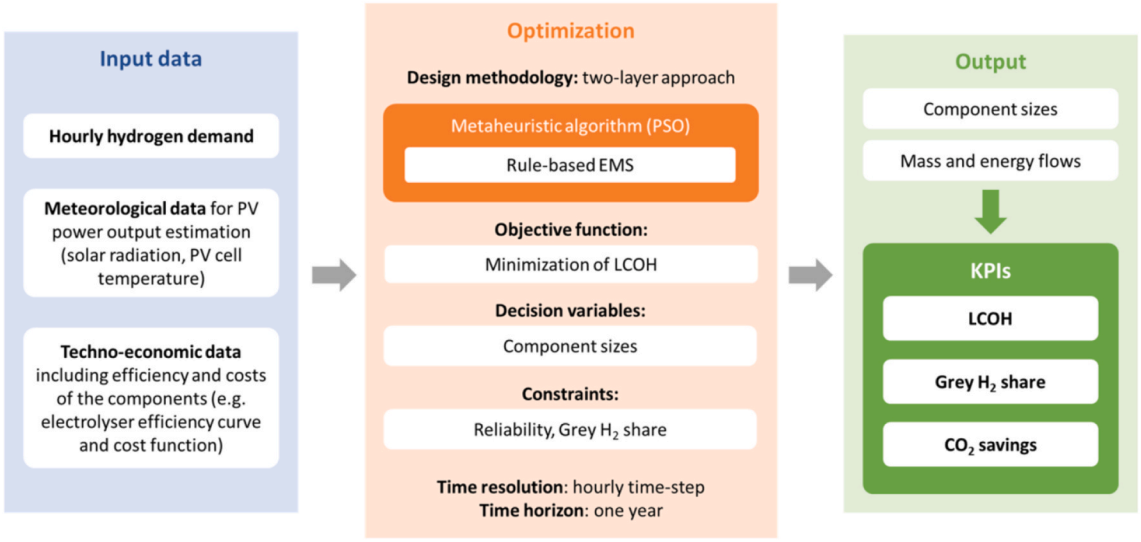

Fig. 2. Optimization framework for the optimal sizing of the power-to-hydrogen system.

hydrogen, grey hydrogen share and CO_2 savings).

The optimal sizing of the system was performed by employing the particle swarm optimization (PSO) algorithm, which is one of the most frequently used metaheuristic methods in the techno-economic optimization of RES-based energy systems. PSO is easy to implement, requiring fewer parameters to tune compared to other optimization techniques, such as genetic algorithms [38]. Moreover, it offers high convergence speed, even for problems with multiple design variables [39] and it is slightly less influenced by the initial solution compared to other metaheuristic methods [40]. Overall, PSO has proven to be a robust optimization technique with strong convergence and stability. In this study, the PSO algorithm was configured with a population size of 100, in agreement with previous study [41,42]. Both the self- and social-adjustment coefficients were set to 1.9 [43], while the inertia factor was set to 0.3 based on the results of a convergence study.

A two-layer approach was implemented to decouple the sizing and the dispatch problems. In the outer loop the PSO algorithm iteratively conducts the sizing procedure to determine the optimal size of the components, while in the inner loop the EMS described in Section 2.1 regulates the operation of the power-to-hydrogen system. The general structure of the optimization problem is summarized below:

$$\begin{aligned} &\min(LCOH) \\ &\text{s.t.:} \\ &\begin{cases} C1: UH_2 \le UH_{2,target} \\ C2: GH_2 \le GH_{2,target} \end{cases} \end{aligned} \tag{1}$$

The optimal design problem thus consists in identifying the set of the decision variables (i.e., the size of the components) that minimizes the levelized cost of hydrogen while satisfying the reliability constraint C1 (which ensures that the unmet hydrogen demand UH_2 is below the threshold $UH_{2,target}$) and the decarbonization constraint C2 (which sets a limit, $GH_{2,target}$, on the use of grey hydrogen, GH_2, in the industrial process).

The size of each component was forced to range between a lower ($S_{i,min}$) and an upper ($S_{i,max}$) bound (with i = PV, EL, HT):

$$S_{i,min} \le S_i \le S_{i,max} \tag{2}$$

The $S_{i,min}$ was set to zero and the $S_{i,max}$ values were chosen in order not to be a limit for the optimal design procedure.

The LCOH (in €/kg), which represents the objective function to be minimized, was defined as follows:

$$LCOH = \frac{C_{NPC,tot}}{\sum_{n=1}^{N} \frac{M_{H_2}}{(1+d)^n}} \tag{3}$$

where $C_{NPC,tot}$ (in €) is the total net present cost (NPC) of the system, M_{H_2} (in kg) is the annual hydrogen demand of the industrial site, d is the real interest rate (set equal to 5 %) and N is the system lifetime (set equal to 20 years).

The NPC includes the capital expenditure (CAPEX), the operation and maintenance (O&M) costs and the replacement costs incurred over the whole lifetime of the system. The NPC was evaluated as (with i = PV, EL, HT, CP):

$$C_{NPC,tot} = \sum_i C_{inv,i} + \sum_{n=1}^{N} \left(\frac{\sum_i C_{O\&M,i,n} + \sum_i C_{rep,i,n} + C_{greyH_2,n} - C_{GR,sell,n}}{(1+d)^n} \right) \tag{4}$$

where $C_{inv,i}$ is the investment cost (i.e., CAPEX) of the i-th component incurred at the beginning of the project, $C_{O\&M,i,n}$ is the operation and maintenance cost of the i-th component during the n-th year, $C_{rep,i,n}$ is the replacement cost of the i-th component incurred at the n-th year (if required), $C_{greyH_2,n}$ is the annual cost due to the purchase of the fossil-based hydrogen and $C_{GR,sell,n}$ is the annual revenue for exporting the surplus PV electricity to the grid (assuming a selling price of 36 €/MWh, which corresponds to approximately 40 % of the electricity purchase price for non-household medium size consumers before 2022 [44,45]).

In Eq. (1), C1 defines the reliability constraint for the power-to-hydrogen system. The UH_2 term is computed as the ratio between the annual uncovered hydrogen demand and the total annual hydrogen consumption:

$$UH_2 = \frac{\sum_{t=1}^{T} (\dot{m}_{H_2,NS}(t) \cdot \Delta t)}{\sum_{t=1}^{T} (\dot{m}_{H_2}(t) \cdot \Delta t)} \tag{5}$$

where $\dot{m}_{H_2,NS}$ (in kg/h) is the hourly unmet hydrogen demand, $\dot{m}_{H_2}$ (in kg/h) is the hourly hydrogen consumption, Δt (in h) is the duration of the time step (i.e., 1 h) and T is the number of time steps in the selected time-horizon (i.e., 8760 h, corresponding to 1 year). To ensure the continuous hydrogen supply to the industrial plant, the target for the unmet hydrogen demand ($UH_{2,target}$) was imposed to zero.

In Eq. (1), C2 specifies the maximum share of grey hydrogen that can

be used in the process. The GH_2 term is defined as the ratio between the annual grey hydrogen use and the total annual hydrogen consumption:

$$GH_2 = \frac{\sum_{t=1}^{T} \left(\dot{m}_{H_2,grey}(t) \cdot \Delta t\right)}{\sum_{t=1}^{T} \left(\dot{m}_{H_2}(t) \cdot \Delta t\right)} \tag{6}$$

where $\dot{m}_{H_2,grey}$ (in kg/h) is the hourly hydrogen demand met by the fossil-based solution. In this work, the $GH_{2,target}$ term was varied to investigate different decarbonization targets and build up a Pareto front according to the ε-constraint method [41,46]. This technique was adopted to minimize both the LCOH and the use of grey hydrogen in the system. Specifically, the multi-objective problem was addressed by optimizing a single objective function and considering the other as an additional constraint. First, two single-objective optimization problems were solved to identify the upper ($GH_{2,max}$) and lower ($GH_{2,min}$) bounds for the grey hydrogen share.

In order to determine the $GH_{2,max}$, a cost-minimization problem was considered without imposing any constraint on the grey hydrogen share:

$$\begin{aligned} &\min(LCOH) \\ &\text{s.t.:} \\ &C1: UH_2 \leq UH_{2,target} \end{aligned} \tag{7}$$

Conversely, the $GH_{2,min}$ value was evaluated by minimizing the fossil-based hydrogen consumption independently of the LCOH:

$$\begin{aligned} &\min(GH_2) \\ &\text{s.t.:} \\ &C1: UH_2 \leq UH_{2,target} \end{aligned} \tag{8}$$

The interval between $GH_{2,max}$ and $GH_{2,min}$ was then divided into multiple segments and for each of them an optimization problem was formulated according to the general structure of Eq. (1). The Pareto front was thus determined through the resolution of a set of single-objective optimizations in which the LCOH is minimized, and the grey hydrogen share is progressively reduced.

Furthermore, to verify the accuracy of the results obtained by using the PSO algorithm combined with the ε-constraint technique, the cost-optimal design was also carried out by adopting a multi-objective genetic algorithm (MOGA) approach. The formulation of the multi-objective problem is reported in Appendix B.

2.3. Components modeling

2.3.1. PV system

The PV power production was estimated as follows [41]:

$$P_{PV}(t) = f_{PV} \cdot P_{PV,rated} \cdot \left(\frac{G_T(t)}{G_{STC}}\right) \cdot \left[1 + \alpha_P \cdot \left(T_c(t) - T_{c,STC}\right)\right] \tag{9}$$

where P_{PV} (in kW) is the output power produced by the PV system, $P_{PV,rated}$ (in kW) is the rated power of the PV system, G_T (in kW/m^2) is the solar radiation incident on the optimally oriented PV panel, G_{STC} (in kW/m^2) is the solar irradiance at Standard Test Conditions (STC), T_c (in °C) is the PV cell temperature during operation, $T_{c,STC}$ (in °C) is the cell temperature at STC, α_P (in 1/K) is the temperature coefficient of power, and f_{PV} is the derating factor.

The PV system performance was modeled using data from a representative commercial monocrystalline panel [47]. The meteorological data needed to assess the PV power production were sourced from the Photovoltaic Geographical Information System (PVGIS), considering the typical meteorological year (TMY) dataset [48]. The PV generation profile was normalized by the nominal power of a single PV panel and used as input data for the optimization code.

A specific investment cost of 800 €/kW was used for the PV system, in accordance with data from utility-scale projects in Europe [49]. The annual O&M cost was set to 2 % of the CAPEX and the lifetime of the system was assumed to be 20 years.

The techno-economic input data of the PV system are summarized in Table 1.

2.3.2. Electrolyzer

A proton exchange membrane (PEM) electrolyzer was adopted for hydrogen production.

This technology is particularly well-suited for integration with variable renewable energy sources, as it can operate effectively under dynamic conditions, offering short start-ups [50], rapid response times [51], and a wide modulation range [52]. These characteristics enable efficient coupling with intermittent power inputs such as solar or wind [53]. Moreover, while dynamic operation may raise concerns regarding accelerated degradation, the lack of extensive data from industrial-scale systems currently limits the ability to accurately quantify these effects [54]. However, recent studies have suggested that dynamic operation does not inherently reduce PEM electrolyzer lifetime. Specifically, some works have reported lower degradation under fluctuating conditions compared to continuous operation [53,55], and even partial recovery effects during resting periods [56].

The efficiency curve shown in Fig. 3a was utilized for modeling the operation of the PEM electrolyzer. The efficiency was defined as the ratio between the hydrogen produced (based on its lower heating value, LHV) and the inlet electrical power to the electrolyzer system (both stack and auxiliaries). It is equal to 55 % under rated conditions and reaches 65 % when the electrolyzer runs at approximately 20 % of the rated power [31]. As shown in Eq. (10), a modulation range was also imposed for the electrolyzer operation:

$$P_{EL,min} \leq P_{EL}(t) \leq P_{EL,rated} \tag{10}$$

where P_{EL} (in kW) is the electrolyzer operating power, $P_{EL,min}$ (in kW) is the minimum electrolyzer operating power and $P_{EL,rated}$ (in kW) is the electrolyzer rated power. In particular, the electrolyzer was assumed to operate between 10 % and 100 % of its rated capacity [31]. Indeed, at lower partial loads, the hydrogen crossover can generate dangerous gas mixtures, and moreover the energy consumption of the balance-of-plant (BOP) components can negatively affect the electrolyzer performance. The modulation range was thus imposed in order to guarantee the safe and efficient operation of the system. Finally, the electrolyzer was assumed to produce pressurized hydrogen at 30 bar (which represents a state-ot-the-art feature for commercial PEM devices).

The specific CAPEX ($c_{inv,EL}$, in €/kW) of the PEM electrolyzer was estimated based on the cost function proposed by Reksten et al. [57]:

$$c_{inv,EL} = \left(k_0 + \frac{k}{P_{EL,rated}} \cdot \left(P_{EL,rated}\right)^{\alpha}\right) \cdot \left(\frac{V}{V_0}\right)^{\beta} \tag{11}$$

where k_0 and k are the fitting parameters, $P_{EL,rated}$ (in kW) is the rated power of the electrolyzer, α is the scaling factor, β is the learning rate, V and V_0 are the plant installation year and the reference year, respectively. The power law reported in Ref. [57] was originally formulated to account for both the influences of plant size and technology maturity, but for the purposes of this study only the size effect was considered.

The term $c_{inv,EL}$ includes the cost of the electrolyzer stack, the balance of plant (BOP) components and the power electronics, but it does not

Table 1
Techno-economic input data of the PV system [41,47,49].

Parameter	Value
f_{PV}	86 %
α_P	−0.003 1/K
Solar irradiance at STC, G_{STC}	1 kW/m^2
Cell temperature at STC, $T_{c,STC}$	25 °C
CAPEX	800 €/kW
O&M (annual)	2 % (of the CAPEX)
Lifetime	20 years

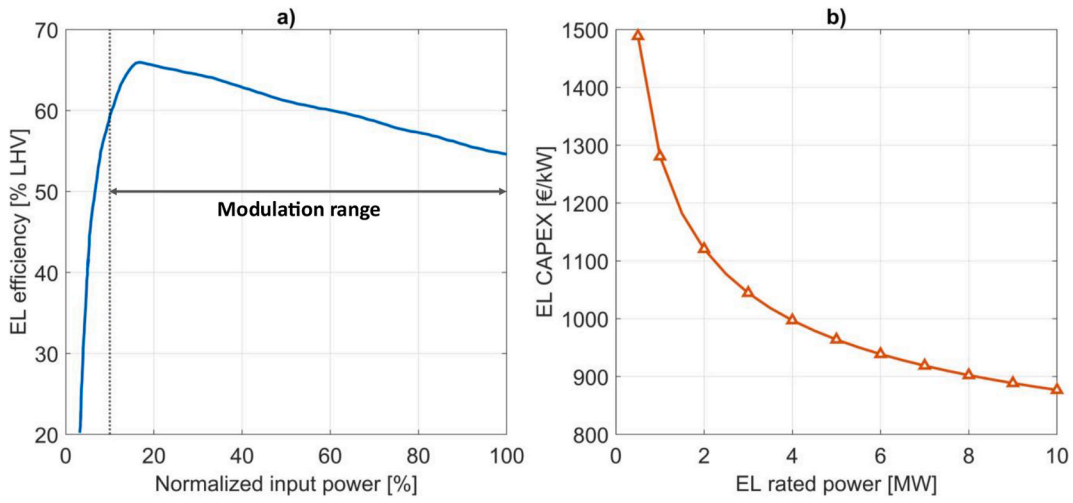

Fig. 3. a) Efficiency curve of the PEM electrolyzer. b) Cost function of the PEM electrolyzer.

account for the installation cost (which was assumed as 10 % of $c_{inv,EL}$). The resulting specific investment cost for PEM electrolyzers in the range of 0.5–10 MW is shown in Fig. 3b.

The replacement cost of the electrolyzer stack was estimated at 26.7 % of the initial investment cost [41], without accounting for projected cost reductions over time, in line with a conservative approach. The stack lifetime was assumed equal to 40,000 h [58] and the replacement year for the electrolyzer stack was determined based on the actual number of operating hours throughout the year, according to the results of the energy simulation for the power-to-hydrogen plant. Finally, the annual O&M cost was set at 3 % of the CAPEX [59].

The main techno-economic input data for the modeling of the PEM electrolyzer are summarized in Table 2.

2.3.3. Hydrogen compression and storage

A hydrogen storage tank was included in the system to provide flexibility and cope with the variable PV production throughout the year. A Type-I tank (i.e., made of seamless aluminum or steel) with a maximum storage pressure of 200 bar was considered.

At each time step, the level of hydrogen (LOH) in the tank, which is defined as the ratio between the amount of hydrogen stored in the tank and its maximum capacity, was updated as follows:

$$LOH(t+1) = LOH(t) + \frac{P_{EL}(t)\cdot\Delta t\cdot\eta_{EL}}{LHV_{H_2}\cdot Cap_{H_2}} - \frac{\dot{m}_{H_2}(t)\cdot\Delta t}{Cap_{H_2}} \quad (12)$$

where η_{EL} is the efficiency of the electrolyzer, LHV_{H_2} (in kWh/kg) is the lower heating value of hydrogen, Cap_{H_2} (in kg) is the rated capacity of the hydrogen tank, and $\dot{m}_{H_2}$ (in kg/h) is the hydrogen demand of the industrial plant.

At each time step, the control strategy must also satisfy the following constraint:

$$LOH_{min} \leq LOH(t) \leq LOH_{max} \quad (13)$$

The LOH_{min} can be evaluated as the ratio between the minimum (i.e., 20 bar) and the maximum storage pressure, while LOH_{max} is equal to 1.

A specific CAPEX of 500 €/kg_{H2} was considered for the pressurized tank, in line with the costs of Type-I tanks with storage pressure below 250 bar [60]. As reported in Section 2.3.2, the electrolyzer produces hydrogen at 30 bar. A three-stage intercooled compressor was thus selected to increase the pressure up to the value of the storage tank. The specific energy consumption was assumed to be 4 MJ/kg for compressing hydrogen from the operating conditions of the electrolyzer up to the maximum storage pressure [61]. The specific investment cost for the compressor was assumed to be 1600 €/kW [61].

The techno-economic input data of the hydrogen compression and storage system are summarized in Table 3.

2.3.4. Grey hydrogen back-up system

A fossil-based back-up solution was also included in the system. Specifically, a tube trailer with pressurized grey hydrogen was considered. The grey hydrogen purchase cost was set at 4 €/kg for the reference scenario [36] and the carbon intensity was assumed equal to 9.5 kg_{CO2}/kg_{H2} [62]. Additionally, a sensitivity analysis on the purchase price of grey hydrogen was conducted to assess its impact on the optimal design of the P-t-H system.

2.4. Case study

In this study, a semiconductor production facility located in Southern

Table 2
Techno-economic input data of the PEM electrolyzer [31,41,57–59].

Parameter	Value
Nominal efficiency ($\eta_{EL,rated}$)	55 %
Modulation range	10–100 % (of the rated power)
Operating pressure	30 bar
α	0.622
β	−158.99
k_0	585.85
k	9458.2
V_0	2020
Installation cost	10 % (of the CAPEX)
O&M (annual)	3 % (of the CAPEX)
Stack replacement cost	26.7 % (of the CAPEX)
Stack lifetime	40,000 h
Balance of plant lifetime	20 years

Table 3
Techno-economic input data for hydrogen compression and storage system [60,61].

Parameter	Value
Hydrogen tank	
Maximum pressure	200 bar
CAPEX	500 €/kgH_2
O&M (annual)	2 % (of the CAPEX)
Lifetime	20 years
Hydrogen compressor	
Specific energy consumption	4 MJ/kgH_2
CAPEX	1600 €/kW
O&M (annual)	2 % (of the CAPEX)
Lifetime	20 years

Europe was considered [63]. The plant operates almost uninterruptedly over the year with a relatively stable hydrogen consumption. The average hydrogen demand is about 12.5 kg/h (in agreement with other literature sources [36]) while the maximum value reaches 15.5 kg/h. The real hourly demand profile of the semiconductor industrial plant was used in this analysis, but further details are omitted for confidentiality reasons. The total annual hydrogen consumption accounts for approximately 110 tonnes and it is currently met by grey hydrogen, which is purchased externally and delivered by trailer.

3. Results

3.1. Baseline scenario

The optimization procedure was first conducted without setting any constraint on the grey hydrogen share ($GH_{2,target}$). The cost-optimal configuration, with an LCOH of 4 €/kg, does not include the installation of the P-t-H system, thus confirming that fossil-based hydrogen currently represents the most cost-effective solution. However, it should be noted that relying completely on grey hydrogen leads to the release of 1045 tonnes of CO_2 per year. The optimal design was then performed by applying the ε-constraint method (described in Section 2.2) and imposing a decreasing limit on the annual grey hydrogen consumption. With the aim of investigating the effect of different decarbonization targets, the $GH_{2,target}$ was varied from 100 % (i.e., current scenario) to 0 % (i.e., fully decarbonized scenario). The sizing results and the main economic and environmental KPIs are summarized in Table 4 and discussed in the following paragraphs.

In Fig. 4, the Pareto front depicts the LCOH trend as a function of the grey hydrogen share. Starting from the current scenario (marked by the red triangle), the LCOH steadily escalates from 4 €/kg to 6.10 €/kg (53 % cost increase) as the annual grey hydrogen share is progressively reduced to 30 %, which corresponds to a decarbonization target of 70 %. Conversely, at higher decarbonization targets (>70 %), the Pareto front exhibits a steeper slope, with the LCOH rising markedly up to 10.51 €/kg in the fully decarbonized scenario (163 % cost increase compared to the current configuration). Therefore, the adoption of a RES-based P-t-H system emerges as a more expensive hydrogen supply strategy, but it can lead to substantial CO_2 emission savings. To confirm the robustness of these results, a comparison with the Pareto front obtained using a MOGA approach is provided in Appendix B.

Fig. 5 shows the NPC breakdown for different values of grey hydrogen share. In the existing configuration, the NPC stands at 5.77 M€, including only the expenses for grey hydrogen purchase (grey bars in Fig. 5). Grey hydrogen procurement dominates the NPC when more than 60 % of the annual demand is covered by fossil-based hydrogen. In contrast, when moving to lower carbon configurations (i.e., grey hydrogen share below approximately 50 %), the components of renewable-based P-t-H system account for the largest cost share. As an example, the NPC of the 50 % GH_2 scenario amounts to 8.04 M€, with

Table 4
Sizing results and main economic and environmental KPIs.

Grey H_2 share [%]	PV [MW]	EL [MW]	HT [kg]	CP [kW]	LCOH [€/kg]	CO_2 emissions [t/y]
100 %	–	–	–	–	4.00	1045
90 %	0.64	0.27	–	–	4.44	940
80 %	1.24	0.55	–	–	4.74	836
70 %	1.84	0.83	18	7	5.02	731
60 %	2.40	1.11	59	12	5.30	627
50 %	3.01	1.39	103	21	5.57	522
40 %	3.62	1.67	149	30	5.84	418
30 %	4.27	1.95	197	35	6.11	313
20 %	5.18	2.27	359	41	6.52	209
10 %	6.75	2.76	633	50	7.28	104
0 %	11.27	3.26	4830	59	10.51	–

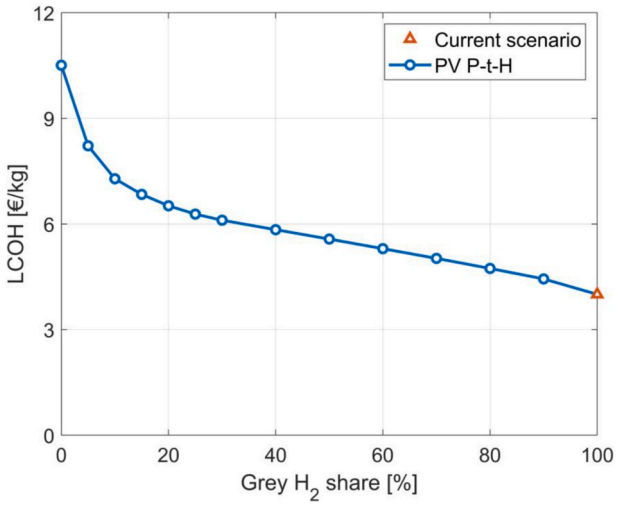

Fig. 4. LCOH of the optimal configuration as a function of the annual grey hydrogen share (Pareto front).

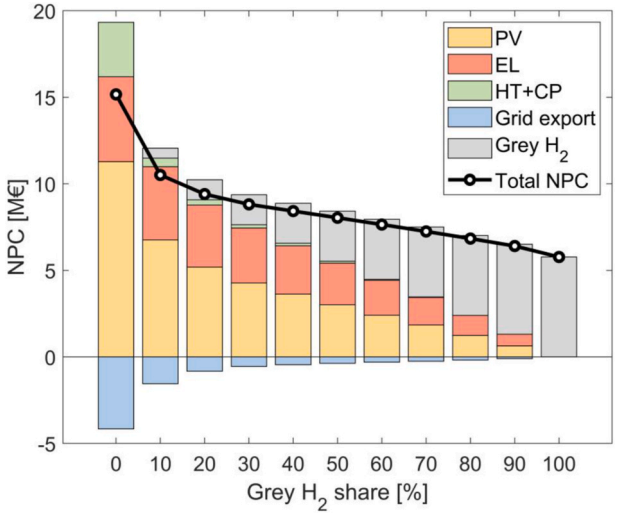

Fig. 5. NPC breakdown for different values of annual grey hydrogen share.

the PV and hydrogen system (i.e., electrolyzer and storage) contributing for 68.9 % of the total NPC. In this case, selling the PV overproduction to the national grid determines a 4.7 % reduction in the NPC (negative blue bars in Fig. 5). It is worth noting that when the grey hydrogen share falls below about 30 %, the revenues from the sale of excess electricity production become more relevant, accounting for up to 4.16 M€. This is due to a substantial increase in the PV size, which can reach up to 11.27 MW when GH_2 is 0 %. In the fully decarbonized scenario, ensuring a continuous green hydrogen supply to the industrial process requires a significant oversizing of both the PV plant and the hydrogen tank. This clearly affects the NPC, which results in 15.16 M€, with the green hydrogen storage system (green bar in Fig. 5) accounting for 19.9 % of the total NPC.

To further investigate the outcomes of the cost-optimal design, Fig. 6 illustrates the variation in the sizes of the P-t-H components as a function of the grey hydrogen use. Fig. 6a depicts the increase in the electrolyzer rated power as the grey hydrogen share reduces. A steady rising trend can be observed for decarbonization targets up to 80 %. More in detail, each 10 % reduction in the annual grey hydrogen consumption requires an increase in the installed electrolyzer capacity by approximately 0.3 MW. Conversely, the addition of around 0.5 MW is needed to achieve the same percentage reduction when the GH_2 share falls below

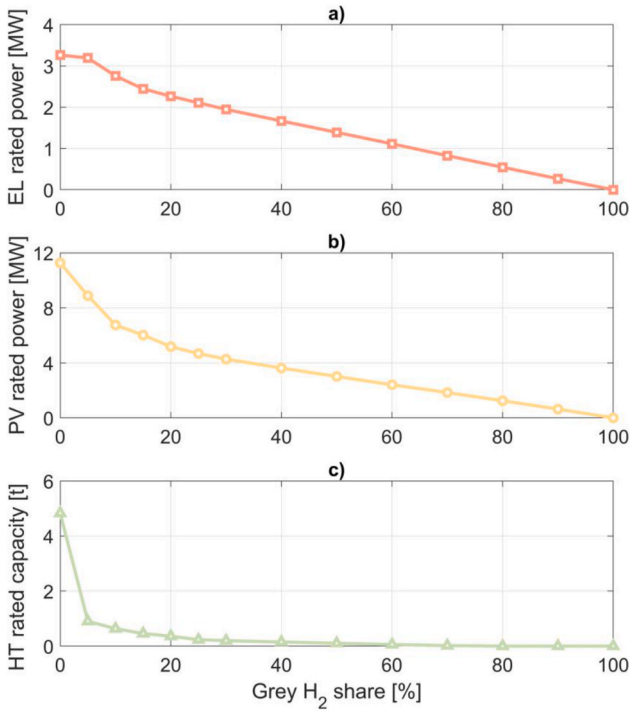

Fig. 6. a) Size of EL for different grey hydrogen shares; b) Size of PV for different grey hydrogen shares; c) Size of HT for different grey hydrogen shares.

approximately 20 %. In the fully decarbonized scenario, the electrolyzer rated power reaches 3.26 MW, which corresponds to a nominal hydrogen production rate of 53.8 kg/h (i.e., 4.3 times larger than the average hourly demand of the plant).

Fig. 6b shows the PV capacity required for the gradual shift towards a fully PV-based hydrogen supply. For GH_2 shares between 100 % and 30 %, the increase in the PV rated power exhibits a linear trend consistent with that of the electrolyzer: a 10 % reduction in the grey hydrogen consumption necessitates 0.6 MW of additional PV capacity. Within this interval, the PV/EL ratio (i.e., the ratio between the rated power of PV and that of the electrolyzer) thus remains nearly stable at around 2.2 and the PV system ensures approximately 3500 h of electrolyzer operation. As the share of grey hydrogen falls below 20 %, the PV rated capacity rises sharply, exceeding 11 MW in the fully decarbonized scenario. This results in a PV/EL ratio of 3.46, which aligns with the values reported for 100 % PV-based P-t-H systems by Marocco et al. [44] and Vincenti et al. [64]. Oversizing the PV system is crucial to avoid reliance on grey hydrogen-based backup and to extend the annual operating time of the electrolyzer, which reaches 3728 h in the fully PV-based scenario.

Fig. 6c reveals that hydrogen storage is not cost-effective in scenarios with heavy reliance on fossil-based hydrogen. However, the installation of pressurized storage becomes profitable when the share of grey hydrogen is less than 70 %. When GH_2 is in the range of 70 %–30 %, the hydrogen tank capacity remains below 200 kg. Achieving more ambitious decarbonization targets requires the integration of larger storage systems. Specifically, the tank size exceeds 600 kg at 10 % GH_2 and increases sharply to 4830 kg in the complete decarbonized scenario, in which the tank oversizing is crucial to manage the mismatch between intermittent PV production and continuous hydrogen demand.

3.2. Impact of grey hydrogen price

A sensitivity analysis on the purchase price of grey hydrogen was conducted to assess its impact on the optimal configuration of the P-t-H system. A price range between 4 and 14 €/kg was explored, as shown in Fig. 7. The conventional hydrogen supply (i.e., 100 % GH_2 scenario)

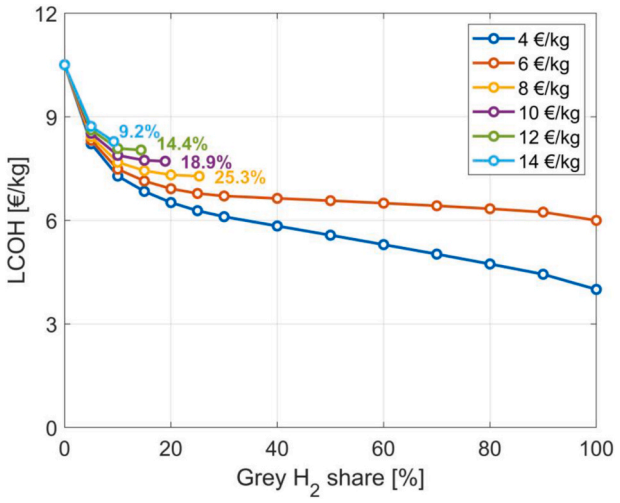

Fig. 7. Pareto fronts for different grey hydrogen prices.

remains the most cost-effective solution for grey hydrogen prices up to 6 €/kg. However, the integration with on-site green hydrogen production becomes cost-efficient when the grey hydrogen purchase cost reaches 8 €/kg, as confirmed by the cost-optimal GH_2 standing at 25.3 %. It is noteworthy that rising grey hydrogen prices determine a progressive reduction in the grey hydrogen share of the cost-optimal configuration, which falls below 20 % for 10 €/kg and decreases to less than 10 % for 14 €/kg. Partially relying on fossil-based hydrogen, even when its cost exceeds 10 €/kg, thus proves to be economically advantageous as it avoids the need to excessively oversize the P-t-H system (particularly the PV plant and hydrogen tank). Additionally, it can be noted that the influence of the grey hydrogen price on the LCOH tends to reduce when moving to lower values of grey hydrogen share. Indeed, the distance between the different Pareto fronts progressively narrows until the optimal design solutions converge to the same design point in the fully decarbonized scenario.

3.3. Impact of grid electricity price

The previous results confirmed that transitioning towards a fully decarbonized hydrogen supply implies substantial cost increase (up to +163 %) and significant system oversizing, particularly in PV and storage units. To reduce or avoid reliance on grey hydrogen backup, while still ensuring supply continuity, the potential benefits of integrating the electrical grid into the P-t-H system were therefore explored. Building upon the baseline system illustrated in Fig. 1, in this extended configuration the electrolyzer can be powered either by the on-site PV plant or by electricity purchased from the grid.

The hybrid PV-grid configuration was examined for the 0 % GH_2 scenario and electricity purchase prices in the range of 50–200 €/MWh were considered. When investigating the hybrid PV-grid configuration for the fully decarbonized scenario, electricity imported from the grid is assumed to be fully renewable, based on contractual mechanisms such as guarantees of origin (GoO) or PPAs, and is therefore considered to have zero associated CO_2 emissions.

The EMS described in Section 2.1 was suitably modified to integrate the possibility of drawing electricity from the grid when PV-based hydrogen production and hydrogen storage are insufficient to meet the demand. Accordingly, the cost-optimal design methodology presented in Section 2.2 was properly adapted to include in the NPC the annual expense for the grid electricity import.

Fig. 8a illustrates the economic KPIs (i.e., NPC breakdown and LCOH) of the hybrid PV-grid P-t-H system importing electricity at different prices. For the sake of comparison, Fig. 8b summarizes the results of the 100 % PV-based configuration.

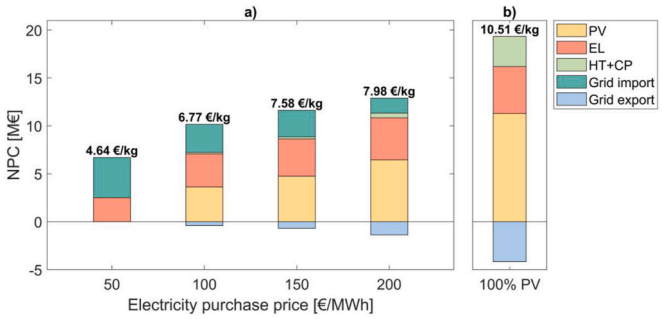

Fig. 8. A comparison of NPC breakdown and LCOH between PV-grid and 100 % PV-based P-t-H system configurations. These results refer to the $GH_2 = 0$ % scenario.

In case of electricity import at 50 €/MWh, the installation of PV power is not included in the optimal solution and a 990 kW electrolyzer runs continuously driven by grid electricity. The LCOH results in 4.64 €/kg (+16 % with respect to the current scenario), which is in line with the values reported by Panah et al. [65] and Terlouw et al. [66] for hydrogen production using low-cost electrical grid supply. A grid-based P-t-H configuration thus emerges as a cost-competitive alternative to conventional grey hydrogen supply, provided that low-cost electricity (such as from PPA or a grid with a high share of renewables) is available. The electricity import dominates the NPC accounting for more than 62.5 %, while the remaining 37.5 % is ascribed to the electrolyzer, primarily due to investment and replacement costs. Indeed, it is worth mentioning that the continuous operation of the electrolyzer determines the frequent stack replacement, which occurs every 5 years (i.e., 3 stack substitutions over the entire system lifetime).

The hydrogen production cost escalates with the electricity purchase price, reaching 7.98 €/kg (+99.5 % compared to the current scenario) at 200 €/MWh. As evident in Fig. 8a, installing PV power becomes cost-effective when the price of grid electricity exceeds 50 €/MWh. In addition, the installed PV capacity grows as the cost of grid supply rises, peaking at 6.45 MW when the electricity purchase price is 200 €/MWh. In this case, a 43 % reduction in the PV rated power can be observed with respect to the PV-based configuration. In the hybrid PV-grid P-t-H systems, the grid connection mitigates the mismatch between PV production and hydrogen demand, thereby limiting the storage size requirements (as confirmed by the minor shares in the NPC breakdown). The hydrogen tank size modestly increases with the electricity purchase price, thus enabling a better exploitation of the PV power production, while remaining considerably smaller compared to the PV-based scenario [67]. More in detail, in case of electricity import at 200 €/MWh, the hydrogen tank capacity results in 627 kg, which is 7.7 times lower than that required in the PV-based configuration.

The grid integration is thus beneficial, even at high electricity prices, since it prevents the oversizing of the P-t-H system components, especially the PV plant and the hydrogen tank, as concluded also by Raab et al. [68].

3.4. Impact of electrolyzer investment cost

The findings from the baseline scenario indicated that achieving complete decarbonization leads to a significant cost increase in the hydrogen supply, largely driven by PV system and electrolyzer contributions. Lower electrolyzer CAPEX could help narrow the cost gap and enhance the economic viability of renewable hydrogen [69]. While PEM electrolyzers offer superior dynamic performance, they are generally associated with higher investment costs than conventional alkaline electrolyzers and emerging anion exchange membrane (AEM) technologies [70,71]. Nevertheless, PEM electrolyzers exhibit higher learning rates compared to mature alkaline technologies and are expected to undergo more significant cost reductions in the coming years [72].

To assess the influence of electrolyzer capital cost on the overall economic performances of the P-t-H system, a sensitivity analysis was carried out by varying the CAPEX of the PEM electrolyzer. In addition to the reference scenario – where a specific CAPEX of 936 €/kW was calculated for an optimized PEM electrolyzer size of 3.26 MW, based on cost function in Eq. (11) – two fixed-CAPEX scenarios were also examined, with specific investment cost set at 1300 €/kW (high CAPEX case) and 660 €/kW (low CAPEX case) [58,73]. This analysis contributes to the generalization of the findings by accounting for cost variability and potential impact of future cost reductions.

Fig. 9 illustrates the impact of electrolyzer capital cost on the LCOH. As expected, a reduction in PEM electrolyzer CAPEX results in a decrease in LCOH. Specifically, the LCOH drops from 11.79 €/kg in the high-CAPEX scenario to 9.49 €/kg in the low-CAPEX scenario, representing a cost reduction of approximately 19.5 %. Moreover, the comparison between the baseline and low-CAPEX scenarios reveals that lowering electrolyzer CAPEX by 29.5 % leads to a reduction in the LCOH by approximately 1 €/kg. Despite the cost reduction achieved in the low-CAPEX scenario, relying entirely on renewable hydrogen remains substantially more expensive than conventional fossil-based hydrogen supply (+137 %). Therefore, while cost improvements in electrolysis technology are essential, they must be complemented by additional technological and economic measures (e.g., improved durability and incentives) to effectively close the cost gap with conventional fossil-based hydrogen.

4. Conclusions

This work aims to investigate the cost-competitiveness of decarbonizing semiconductor manufacturing by switching from conventional grey hydrogen supply to on-site green hydrogen production through a PV-based P-t-H system. An optimization framework based on a meta-heuristic approach was developed for the optimal sizing of the P-t-H system and the ε-constraint technique was adopted to explore different decarbonization targets. Additionally, a sensitivity analysis on the grey hydrogen purchase price was carried out to assess its impact on the optimal system sizing. The main findings of the work are summarized as follows:

- At present, relying completely on grey hydrogen remains the cost-optimal supply strategy (LCOH of 4 €/kg), but it results in the emission of 1045 tonnes of CO_2 per year. When progressively reducing the grey hydrogen consumption, the LCOH increases until peaking at 10.51 €/kg (+163 % compared to the current solution) in the fully decarbonized scenario. Thus, installing a PV-based P-t-H system proves to be more expensive, but it effectively limits the CO_2 emissions associated with the hydrogen supply.

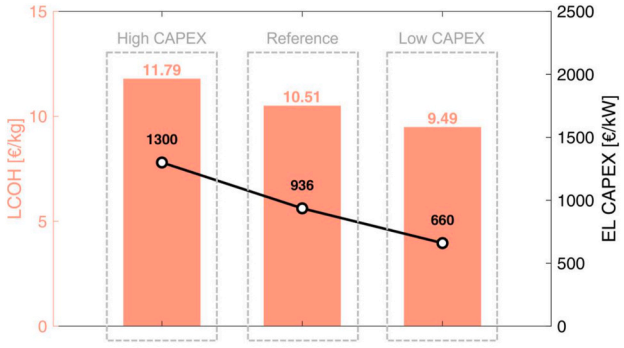

Fig. 9. Effect of electrolyzer investment cost (EL CAPEX) on the LCOH. The "reference" case corresponds to the cost of the PEM electrolyzer used in previous sections, computed via Eq. (11) for the optimal PEM sizing (3.26 MW).

- Limiting the use of grey hydrogen necessitates an increase in the size of the P-t-H components. To achieve ambitious decarbonization targets (i.e., GH_2 lower than 30 %), a sharp rise in the sizes of the PV plant, electrolyzer and hydrogen storage is necessary. Complete decarbonization requires a PV rated power exceeding 11 MW and an electrolyzer rated power of 3.26 MW. In this scenario, the hydrogen tank size must increase to 4830 kg to address the mismatch between intermittent PV production and continuous hydrogen demand.
- When grey hydrogen is used to fulfill over 60 % of the annual hydrogen demand, its procurement dominates the NPC. Conversely, in low-emission configurations, the components of the P-t-H system represent the largest cost shares. In the fully decarbonized scenario, the hydrogen tank is significantly oversized to guarantee a reliable hydrogen supply, accounting for 19.9 % of the overall NPC.
- Fossil-based hydrogen supply remains cost-efficient at grey hydrogen prices up to 6 €/kg. Beyond this threshold, integrating on-site green hydrogen production becomes beneficial, and the maximum grey hydrogen share in the cost-optimal solution gradually reduces as the grey hydrogen price rises.
- When importing electricity at 50 €/MWh, the PV power installation is not cost-effective and the electrolyzer thus operates continuously driven by the grid. Low-cost electricity thus leads to an LCOH of 4.64 €/kg, which is comparable with the cost of conventional hydrogen supply. In case of hybrid PV-grid power supply, the LCOH varies with the electricity purchase price and lies in the range of 6.77–7.98 €/kg. The grid integration, even at high electricity prices, thus enhances the competitiveness of green hydrogen production as it prevents the oversizing of PV system and hydrogen tank.
- While lowering the electrolyzer CAPEX by 29.5 % improves the economic performance of the P-t-H system by reducing the LCOH of approximately 1 €/kg, additional technological improvements and supportive regulatory frameworks are required to achieve the cost-parity with conventional hydrogen supply.

While this study considers a relatively small hydrogen demand (110 tonnes/year) and CO_2 emissions (1045 tonnes/year), it offers valuable insights into early-stage deployment of renewable hydrogen in a specialized industrial setting, in which fossil-based hydrogen supply can be readily replaced without major process modifications. Building on this case, the proposed methodology is designed to be scalable and adaptable to other industrial applications, including larger and more complex hard-to-abate sectors. Future works will apply this framework to evaluate the profitability of adopting green hydrogen in hard-to-abate industries, such as refining, ammonia synthesis and glass production. Additionally, the impact of the grid integration will be explored in greater detail, and alternative power supply schemes, (e.g., as produced PPAs) will be investigated.

CRediT authorship contribution statement

Davide Trapani: Writing – original draft, Visualization, Software, Resources, Methodology, Investigation, Formal analysis, Data curation, Conceptualization. **Paolo Marocco:** Writing – review & editing, Visualization, Supervision, Resources, Methodology, Formal analysis, Data curation, Conceptualization. **Marta Gandiglio:** Writing – review & editing, Visualization, Supervision, Resources, Methodology, Formal analysis, Data curation, Conceptualization. **Massimo Santarelli:** Writing – review & editing, Supervision, Project administration, Funding acquisition.

Declaration of generative AI and AI-assisted technologies in the writing process

During the preparation of this work the authors used ChatGPT in order to improve the readability of the manuscript. After using this tool, the authors reviewed and edited the content as needed and take full responsibility for the content of the publication.

Declaration of competing interest

The authors declare that they have no known competing financial interests or personal relationships that could have appeared to influence the work reported in this paper.

Acknowledgements

The work has been conducted in the framework of the IMAGHYNE (Investment to maximise the ambition for green hydrogen in Europe) project (https://cordis.europa.eu/project/id/101137586). The project is supported by the Clean Hydrogen Partnership and its members (GA: 101137586).

Funded by the European Union - NextGenerationEU, Mission 4 Component 2 - ECS00000036 – CUP [E13B22000020001].

Acronyms

BF-BOF	Blast furnace-Basic oxygen furnace
BOP	Balance of plant
CAPEX	Capital expenditures
CP	Compressor
DRI	Direct reduced iron
EL	Electrolyzer
EMS	Energy management strategy
GoO	Guarantee of origin
GR	Grid
HBS	Hydrogen back-up system
HT	Hydrogen tank
IEA	International Energy Agency
IRENA	International Renewable Energy Agency
KPI	Key performance indicator
LCOA	Levelized cost of ammonia
LCOH	Levelized cost of hydrogen
LCOM	Levelized cost of methanol
LHV	Lower heating value
LOH	Level of hydrogen
MOGA	Multi-objective genetic algorithm
NPC	Net present cost
O&M	Operation and maintenance

(*continued on next page*)

(*continued*)

OPEX	Operational expenditures
PEM	Proton exchange membrane
PPA	Power purchase agreement
PSO	Particle swarm optimization
P-t-H	Power-to-hydrogen
PV	Photovoltaic
PVGIS	Photovoltaic geographic information system
RES	Renewable energy sources
SMR	Steam methane reforming
SOE	Solid oxide electrolyzer
STC	Standard test conditions
TMY	Typical meteorological year

Appendix A. Logical block diagram of the energy management strategy

Figure A.1 shows the logical block diagram of the energy management strategy developed to regulate the operation of the renewable P-t-H system.

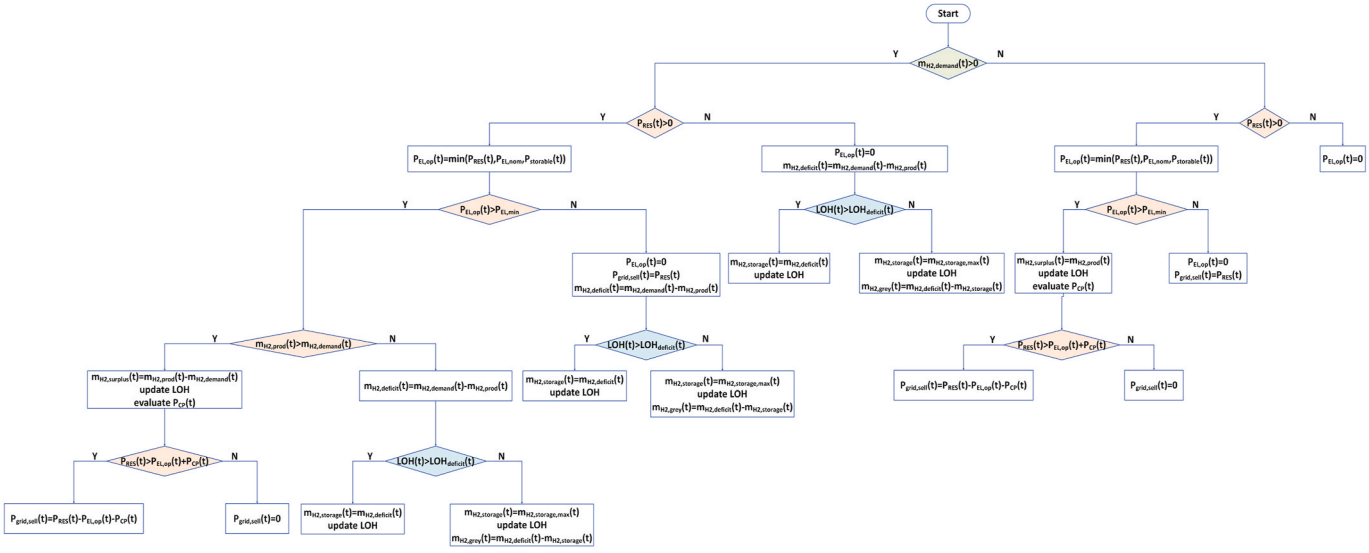

Fig. A.1. Logical block diagram of the EMS.

The nomenclature adopted in the control strategy is reported in Table A.1.

Table A.1
Nomenclature adopted in the logic block diagram of the EMS.

Symbol	Definition
GH_2	Grey hydrogen share
$LOH_{deficit}(t)$	LOH required to cover the hourly hydrogen deficit
$m_{H2,demand}(t)$	Hourly hydrogen demand
$m_{H2,prod}(t)$	Hourly hydrogen production
$m_{H2,surplus}(t)$	Hourly hydrogen surplus
$m_{H2,deficit}(t)$	Hourly hydrogen deficit
$m_{H2,storage}(t)$	Hourly hydrogen demand covered by the storage
$m_{H2,storage,max}(t)$	Maximum amount of hydrogen available in the storage
$m_{H2,grey}(t)$	Hourly hydrogen demand covered by grey hydrogen
$P_{RES}(t)$	Electrical power produced from RES
$P_{EL,op}(t)$	Electrolyzer operating power
$P_{EL,nom}(t)$	Electrolyzer nominal power
$P_{EL,min}$	Electrolyzer minimum operating power
$P_{storable}(t)$	Maximum electrolyzer operating power to not to exceed LOH_{max}
$P_{CP}(t)$	Compressor power
$P_{grid,sell}(t)$	Electrical power sold to the grid
UH_2	Unmet hydrogen demand
$UH_{2,target}$	Unmet hydrogen demand target

Appendix B. Multi-objective optimization and MOGA approach

The multi-objective optimization problem is formulated as follows:

$$\begin{aligned} &\min(LCOH, GH_2) \\ &\text{s.t.:} \\ &C1: UH_2 \leq UH_{2,target} \end{aligned} \tag{B.1}$$

In this case, both objective functions (i.e., LCOH and grey hydrogen share) are simultaneously minimized while satisfying the reliability constraint C1.

When solving the optimization problem with the MOGA approach, a population size of 150 individuals and a crossover fraction of 0.8 were adopted [74,75].

Figure B.1 compares the results obtained when applying the PSO algorithm with ε-constraint technique and the MOGA approach. The good agreement between the Pareto fronts confirms the robustness and consistency of the cost-optimal design methodology.

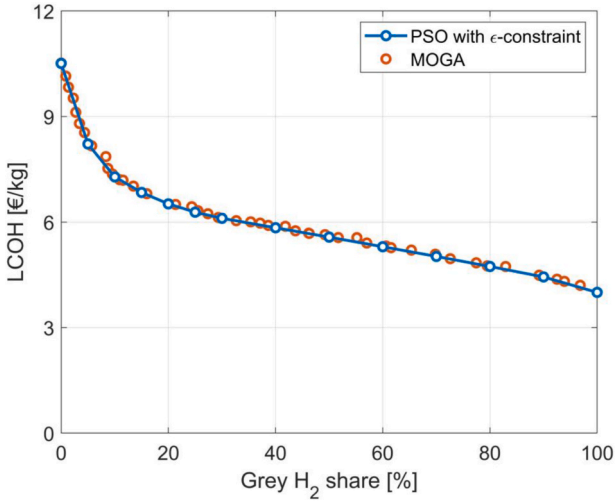

Fig. B.1. Comparison between the Pareto fronts obtained by using PSO with ε-constraint and MOGA.

Data availability

The data that has been used is confidential.

References

[1] International Energy Agency. CO2 emissions in 2022 [Online]. Available: https://www.iea.org/reports/co2-emissions-in-2022. [Accessed 27 June 2025].

[2] International Energy Agency. Achieving net zero heavy industry sectors in G7 members [Online]. Available: https://www.iea.org/reports/achieving-net-zero-heavy-industry-sectors-in-g7-members. [Accessed 22 April 2025].

[3] International Renewable Energy Agency. Green hydrogen for industry: a guide to policy making. Abu Dhabi. 2022 [Online]. Available: https://www.irena.org/Publications/2022/Mar/Green-Hydrogen-for-Industry. [Accessed 22 April 2025].

[4] International Energy Agency. Global hydrogen review 2024 [Online]. Available: https://www.iea.org/reports/global-hydrogen-review-2024. [Accessed 6 April 2025].

[5] International Energy Agency. Global hydrogen review 2023 [Online]. Available: https://www.iea.org/reports/global-hydrogen-review-2023. [Accessed 22 April 2025].

[6] Moradpoor I, Syri S, Santasalo-Aarnio A. Green hydrogen production for oil refining – finnish case. Renew Sustain Energy Rev Apr. 2023;175. https://doi.org/10.1016/j.rser.2023.113159.

[7] Gandhi K, Apostoleris H, Sgouridis S. Catching the hydrogen train: economics-driven green hydrogen adoption potential in the United Arab Emirates. Int J Hydrogen Energy Jun. 2022;47(53):22285–301. https://doi.org/10.1016/j.ijhydene.2022.05.055.

[8] Al-Subaie A, Maroufmashat A, Elkamel A, Fowler M. Presenting the implementation of power-to-gas to an oil refinery as a way to reduce carbon intensity of petroleum fuels. Int J Hydrogen Energy Jul. 2017;42(30):19376–88. https://doi.org/10.1016/j.ijhydene.2017.06.067.

[9] Ferraro M, Massaro F, Sanseverino ER, Ruffino S. Is selling the oxygen produced during electrolysis really a solution to make green hydrogen cheaper?. In: 2024 IEEE international conference on environment and electrical engineering and 2024 IEEE industrial and commercial power systems Europe (EEEIC/I& CPS Europe). IEEE; Jun. 2024. p. 1–6. https://doi.org/10.1109/EEEIC/ICPSEurope61470.2024.10751545.

[10] Bo Z, Said MFM, Erdiwansyah E, Mamat R, Xiaoxia J. A review of oxygen generation through renewable hydrogen production. Sustain Chem Clim Action Jun. 2025;6:100079. https://doi.org/10.1016/j.scca.2025.100079.

[11] Eckl F, Moita A, Castro R, Neto RC. Valorization of the by-product oxygen from green hydrogen production: a review. Appl Energy Jan. 2025;378. https://doi.org/10.1016/j.apenergy.2024.124817.

[12] Assunção R, Eckl F, Ramos CP, Correia CB, Neto RC. Oxygen liquefaction economical value in the development of the hydrogen economy. Int J Hydrogen Energy Apr. 2024;62:109–18. https://doi.org/10.1016/j.ijhydene.2024.02.205.

[13] International Renewable Energy Agency (IRENA) and Methanol Institute. Innovation outlook: renewable methanol. 2021 [Online]. Available: https://www.irena.org/Publications/2021/Jan/Innovation-Outlook-Renewable-Methanol. [Accessed 22 April 2025].

[14] Gu Y, Wang D, Chen Q, Tang Z. Techno-economic analysis of green methanol plant with optimal design of renewable hydrogen production: a case study in China. Int J Hydrogen Energy Jan. 2022;47(8):5085–100. https://doi.org/10.1016/j.ijhydene.2021.11.148.

[15] Sollai S, Porcu A, Tola V, Ferrara F, Pettinau A. Renewable methanol production from green hydrogen and captured CO2: a techno-economic assessment. J CO2 Util 2023;68(Feb). https://doi.org/10.1016/j.jcou.2022.102345.

[16] Mingolla S, et al. Effects of emissions caps on the costs and feasibility of low-carbon hydrogen in the European ammonia industry. Nat Commun May 2024;15(1):3753. https://doi.org/10.1038/s41467-024-48145-z.

[17] Mersch M, et al. A comparative techno-economic assessment of blue, green, and hybrid ammonia production in the United States. Sustain Energy Fuels 2024. https://doi.org/10.1039/d3se01421e.

[18] Standard and Poor's S&P Global, "Interactive: Platts ammonia price chart." Accessed: June. 15, 2025. [Online]. Available: https://www.spglobal.com/commodity-insights/en/news-research/latest-news/energy-transition/051023-interactive-ammonia-price-chart-natural-gas-feedstock-europe-usgc-black-sea.

[19] Magnino A, Marocco P, Santarelli M, Gandiglio M. Economic viability and CO2 emissions of hydrogen production for ammonia synthesis: a comparative analysis across Europe. Adv Appl Energy Mar. 2025;17. https://doi.org/10.1016/j.adapen.2024.100204.

[20] International Renewable Energy Agency and Ammonia Energy Association. Innovation outlook: renewable ammonia. 2022 [Online]. Available: https://www.irena.org/Publications/2022/May/Innovation-Outlook-Renewable-Ammonia. [Accessed 22 April 2025].

[21] Osman O, Sgouridis S, Sleptchenko A. Scaling the production of renewable ammonia: a techno-economic optimization applied in regions with high insolation. J Clean Prod Oct. 2020;271:121627. https://doi.org/10.1016/j.jclepro.2020.121627.

[22] Nami H, Hendriksen PV, Frandsen HL. Green ammonia production using current and emerging electrolysis technologies. Renew Sustain Energy Rev Jul. 2024;199. https://doi.org/10.1016/j.rser.2024.114517.

[23] Wang C, Walsh SDC, Longden T, Palmer G, Lutalo I, Dargaville R. Optimising renewable generation configurations of off-grid green ammonia production systems considering Haber-bosch flexibility. Energy Convers Manag Mar. 2023; 280. https://doi.org/10.1016/j.enconman.2023.116790.
[24] Smith C, Hill AK, Torrente-Murciano L. Current and future role of Haber–Bosch ammonia in a carbon-free energy landscape. Energy Environ Sci 2020;13(2): 331–44. https://doi.org/10.1039/C9EE02873K.
[25] Martinez Alonso A, Naval N, Matute G, Coosemans T, Yusta JM. Phasing out steam methane reformers with water electrolysis in producing renewable hydrogen and ammonia: a case study based on the Spanish energy markets. Int J Hydrogen Energy 2023. https://doi.org/10.1016/j.ijhydene.2023.07.347.
[26] International Energy Agency. Iron and steel technology roadmap towards more sustainable steelmaking [Online]. Available: https://www.iea.org/reports/iron-and-steel-technology-roadmap. [Accessed 22 April 2025].
[27] Vogl V, Åhman M, Nilsson LJ. Assessment of hydrogen direct reduction for fossil-free steelmaking. J Clean Prod Dec. 2018;203:736–45. https://doi.org/10.1016/j.jclepro.2018.08.279.
[28] Bhaskar A, Abhishek R, Assadi M, Somehesaraei HN. Decarbonizing primary steel production: techno-economic assessment of a hydrogen based green steel production plant in Norway. J Clean Prod May 2022;350. https://doi.org/10.1016/j.jclepro.2022.131339.
[29] Elsheikh H, Eveloy V. Assessment of variable solar- and grid electricity-driven power-to-hydrogen integration with direct iron ore reduction for low-carbon steel making. Fuel Sep. 2022;324:124758. https://doi.org/10.1016/j.fuel.2022.124758.
[30] Superchi F, Mati A, Carcasci C, Bianchini A. Techno-economic analysis of wind-powered green hydrogen production to facilitate the decarbonization of hard-to-abate sectors: a case study on steelmaking. Appl Energy Jul. 2023;342. https://doi.org/10.1016/j.apenergy.2023.121198.
[31] Marocco P, Gandiglio M, Audisio D, Santarelli M. Assessment of the role of hydrogen to produce high-temperature heat in the steel industry. J Clean Prod Feb. 2023;388. https://doi.org/10.1016/j.jclepro.2023.135969.
[32] Röben FTC, Schöne N, Bau U, Reuter MA, Dahmen M, Bardow A. Decarbonizing copper production by power-to-hydrogen: a techno-economic analysis. J Clean Prod Jul. 2021;306. https://doi.org/10.1016/j.jclepro.2021.127191.
[33] Neuwirth M, Fleiter T, Manz P, Hofmann R. The future potential hydrogen demand in energy-intensive industries - a site-specific approach applied to Germany. Energy Convers Manag Jan. 2022;252. https://doi.org/10.1016/j.enconman.2021.115052.
[34] Gärtner S, et al. Simulation and techno-economic analysis of a power-to-hydrogen process for oxyfuel glass melting. Energies (Basel) Dec. 2021;14(24). https://doi.org/10.3390/en14248603.
[35] Boudries R, Khellaf A, Aliane A, Ihaddaden L, Khida F. PV system design for powering an industrial unit for hydrogen production. Int J Hydrogen Energy Sep. 2014;39(27):15188–95. https://doi.org/10.1016/j.ijhydene.2014.04.166.
[36] Rochlitz L, et al. Second use or recycling of hydrogen waste gas from the semiconductor industry - economic analysis and technical demonstration of possible pathways. Int J Hydrogen Energy Jun. 2019;44(31):17168–84. https://doi.org/10.1016/j.ijhydene.2019.05.009.
[37] Das BK, Hasan M, Das P. Impact of storage technologies, temporal resolution, and PV tracking on stand-alone hybrid renewable energy for an Australian remote area application. Renew Energy Aug. 2021;173:362–80. https://doi.org/10.1016/j.renene.2021.03.131.
[38] Sharafi M, El Mekkawy TY. Multi-objective optimal design of hybrid renewable energy systems using PSO-simulation based approach. Renew Energy Aug. 2014; 68:67–79. https://doi.org/10.1016/j.renene.2014.01.011.
[39] Destro N, Benato A, Stoppato A, Mirandola A. Components design and daily operation optimization of a hybrid system with energy storages. Energy Dec. 2016; 117:569–77. https://doi.org/10.1016/j.energy.2016.05.097.
[40] Tezer T, Yaman R, Yaman G. Evaluation of approaches used for optimization of stand-alone hybrid renewable energy systems. Elsevier Ltd; 2017. https://doi.org/10.1016/j.rser.2017.01.118.
[41] Marocco P, Ferrero D, Lanzini A, Santarelli M. The role of hydrogen in the optimal design of off-grid hybrid renewable energy systems. J Energy Storage 2022;46 (Feb). https://doi.org/10.1016/j.est.2021.103893.
[42] Marocco P, Ferrero D, Lanzini A, Santarelli M. Optimal design of stand-alone solutions based on RES + hydrogen storage feeding off-grid communities. Energy Convers Manag 2021;238(Jun). https://doi.org/10.1016/j.enconman.2021.114147.
[43] Papazoglou G, Biskas P. Review and comparison of genetic algorithm and particle swarm optimization in the optimal power flow problem. Energies (Basel) Jan. 2023;16(3):1152. https://doi.org/10.3390/en16031152.
[44] Marocco P, Gandiglio M, Santarelli M. Optimal design of PV-based grid-connected hydrogen production systems. J Clean Prod 2024;434(Jan). https://doi.org/10.1016/j.jclepro.2023.140007.
[45] European union - Electricity prices: non-household, medium size consumers [Online]. Available: https://tradingeconomics.com/european-union/electricity-prices-non-household-medium-size-consumers-eurostat-data.html. [Accessed 28 December 2024].
[46] Gabrielli P, Gazzani M, Martelli E, Mazzotti M. Optimal design of multi-energy systems with seasonal storage. Appl Energy Jun. 2018;219:408–24. https://doi.org/10.1016/j.apenergy.2017.07.142.
[47] LG. High efficiency LG NeON® R module LG365Q1C-A5 [Online]. Available: https://www.lg.com/us/business/solar-panels/lg-LG365Q1C-A5. [Accessed 19 March 2025].
[48] Photovoltaic geographical information system [Online]. Available: https://joint-research-centre.ec.europa.eu/pvgis-online-tool_en. [Accessed 8 March 2025].
[49] International Renewable Energy Agency. Renewable power generation costs in 2022. Abu Dhabi, www.irena.org; 2023.
[50] Wang J, Wen J, Wang J, Yang B, Jiang L. Water electrolyzer operation scheduling for green hydrogen production: a review. Renew Sustain Energy Rev Oct. 2024; 203:114779. https://doi.org/10.1016/j.rser.2024.114779.
[51] Crespi E, Guandalini G, Mastropasqua L, Campanari S, Brouwer J. Experimental and theoretical evaluation of a 60 kW PEM electrolysis system for flexible dynamic operation. Energy Convers Manag Feb. 2023;277:116622. https://doi.org/10.1016/j.enconman.2022.116622.
[52] Martinez Lopez VA, Ziar H, Haverkort JW, Zeman M, Isabella O. Dynamic operation of water electrolyzers: a review for applications in photovoltaic systems integration. Elsevier Ltd.; Aug. 01, 2023. https://doi.org/10.1016/j.rser.2023.113407.
[53] Sayed-Ahmed H, Toldy I, Santasalo-Aarnio A. Dynamic operation of proton exchange membrane electrolyzers—Critical review. Elsevier Ltd.; Jan. 01, 2024. https://doi.org/10.1016/j.rser.2023.113883.
[54] Nguyen E, Olivier P, Pera M-C, Pahon E, Roche R. Impacts of intermittency on low-temperature electrolysis technologies: a comprehensive review. Int J Hydrogen Energy Jun. 2024;70:474–92. https://doi.org/10.1016/j.ijhydene.2024.05.217.
[55] Rakousky C, et al. Polymer electrolyte membrane water electrolysis: restraining degradation in the presence of fluctuating power. J Power Sources Feb. 2017;342: 38–47. https://doi.org/10.1016/j.jpowsour.2016.11.118.
[56] Zhang H, Yuan T. Optimization and economic evaluation of a PEM electrolysis system considering its degradation in variable-power operations. Appl Energy Oct. 2022;324. https://doi.org/10.1016/j.apenergy.2022.119760.
[57] Reksten AH, Thomassen MS, Møller-Holst S, Sundseth K. Projecting the future cost of PEM and alkaline water electrolysers; a CAPEX model including electrolyser plant size and technology development. Int J Hydrogen Energy Nov. 2022;47(90): 38106–13. https://doi.org/10.1016/j.ijhydene.2022.08.306.
[58] Matute G, Yusta JM, Beyza J, Monteiro C. Optimal dispatch model for PV-electrolysis plants in self-consumption regime to produce green hydrogen: a Spanish case study. Int J Hydrogen Energy Jul. 2022;47(60):25202–13. https://doi.org/10.1016/j.ijhydene.2022.05.270.
[59] Matute G, Yusta JM, Correas LC. Techno-economic modelling of water electrolysers in the range of several MW to provide grid services while generating hydrogen for different applications: a case study in Spain applied to mobility with FCEVs. Int J Hydrogen Energy Jul. 2019;44(33):17431–42. https://doi.org/10.1016/j.ijhydene.2019.05.092.
[60] Danish Energy Agency. Technology data-energy storage [Online]. Available: http://www.ens.dk/teknologikatalog; 2020.
[61] Crespi E, Colbertaldo P, Guandalini G, Campanari S. Design of hybrid power-to-power systems for continuous clean PV-based energy supply. Int J Hydrogen Energy Apr. 2021;46(26):13691–708. https://doi.org/10.1016/j.ijhydene.2020.09.152.
[62] International Renewable Energy Agency. Hydrogen: a renewable energy perspective. Abu Dhabi. 2019 [Online]. Available: https://www.irena.org/Publications/2019/Sep/Hydrogen-A-renewable-energy-perspective. [Accessed 3 June 2025].
[63] Trapani D, Marocco P, Gandiglio M, Santarelli M. Optimal design of renewable power-to-hydrogen systems for the decarbonization of a semiconductor industry. In: 36th international conference on efficiency, cost, optimization, simulation and environmental impact of energy systems (ECOS 2023). Spain: ECOS: Las Palmas De Gran Canaria; 2023, 2023. p. 2523–31. https://doi.org/10.52202/069564-0227.
[64] Vincenti F, Cominini P, Furlanetto D, Sorlini A, Valenti G. Optimized size and schedule of the power-to-hydrogen system connected to a hydrogen refuelling station for waste transportation vehicles in Valle Camonica. In: *Journal of physics: conference series*, institute of physics; 2022. https://doi.org/10.1088/1742-6596/2385/1/012039.
[65] Ghaebi Panah P, Cui X, Bornapour M, Hooshmand RA, Guerrero JM. Marketability analysis of green hydrogen production in Denmark: scale-up effects on grid-connected electrolysis. Int J Hydrogen Energy Mar. 2022;47(25):12443–55. https://doi.org/10.1016/j.ijhydene.2022.01.254.
[66] Terlouw T, Bauer C, McKenna R, Mazzotti M. Large-scale hydrogen production via water electrolysis: a techno-economic and environmental assessment. Energy Environ Sci Jul. 2022;15(9):3583–602. https://doi.org/10.1039/d2ee01023b.
[67] Stolte M, Minuto FD, Lanzini A. Optimizing green hydrogen production from wind and solar for hard-to-abate industrial sectors across multiple sites in Europe. Int J Hydrogen Energy Aug. 2024;79:1201–14. https://doi.org/10.1016/j.ijhydene.2024.07.106.
[68] Raab M, Körner R, Dietrich RU. Techno-economic assessment of renewable hydrogen production and the influence of grid participation. Int J Hydrogen Energy Jul. 2022;47(63):26798–811. https://doi.org/10.1016/j.ijhydene.2022.06.038.
[69] Bühler L, Möst D. Derivation of one- and two-factor experience curves for electrolysis technologies. Int J Hydrogen Energy Nov. 2024;89:105–16. https://doi.org/10.1016/j.ijhydene.2024.09.243.
[70] Chatenet M, et al. Water electrolysis: from textbook knowledge to the latest scientific strategies and industrial developments. Chem Soc Rev 2022;51(11): 4583–762. https://doi.org/10.1039/D0CS01079K.
[71] Kim M, Lee D, Qi M, Kim J. Techno-economic analysis of anion exchange membrane electrolysis process for green hydrogen production under uncertainty. Energy Convers Manag Feb. 2024;302. https://doi.org/10.1016/j.enconman.2024.118134.
[72] Krishnan S, et al. Present and future cost of alkaline and PEM electrolyser stacks. Int J Hydrogen Energy Oct. 2023;48(83):32313–30. https://doi.org/10.1016/j.ijhydene.2023.05.031.

[73] Dufo-López R, Lujano-Rojas JM, Bernal-Agustín JL. Optimisation of size and control strategy in utility-scale green hydrogen production systems. Int J Hydrogen Energy 2023. https://doi.org/10.1016/j.ijhydene.2023.08.273.
[74] Hassanat A, Almohammadi K, Alkafaween E, Abunawas E, Hammouri A, Prasath VBS. Choosing mutation and crossover ratios for genetic algorithms—A review with a new dynamic approach. Information Dec. 2019;10(12):390. https://doi.org/10.3390/info10120390.
[75] Brka A, Al-Abdeli YM, Kothapalli G. The interplay between renewables penetration, costing and emissions in the sizing of stand-alone hydrogen systems. Int J Hydrogen Energy Jan. 2015;40(1):125–35. https://doi.org/10.1016/j.ijhydene.2014.10.132.